Pergamon

Int. J. Heat Mass Transfer. Vol. 37, No. 3, pp. 387–399, 1994
Copyright © 1994 Elsevier Science Ltd
Printed in Great Britain. All rights reserved
0017-9310/94 $6.00 + 0.00

Numerical study of thermal convection in shallow cavities with conducting boundaries

P. WANG and P. G. DANIELS

Department of Mathematics, City University, Northampton Square, London EC1V 0HB, U.K.

(*Received* 17 *February* 1993 *and in final form* 25 *August* 1993)

Abstract—Two-dimensional convective flows in shallow cavities with conducting horizontal boundaries and driven by differential heating of the two vertical end walls, are studied numerically over a range of Rayleigh numbers and Prandtl numbers. As the Rayleigh number increases, nonlinearity first affects the flow structure in the turning regions near the ends of the cavity. These 'end-zone problems' have been investigated by a combined computational and analytical approach. Numerical solutions are found using a Dufort–Frankel-Multigrid method, and appear to be in good agreement with stability analysis.

1. INTRODUCTION

CONVECTIVE motions driven by lateral temperature gradients in slender cavities are important in many areas of interest in industry and in nature. Applications include the temperature control of circuit board components under natural convection in the electronics industry, heating and ventilation control in building design and construction, cooling systems for reactors in the nuclear industry, flows and heat transfer associated with all stages of the power generation process, solar-energy collectors in the power industry and atmospheric and fluvial dispersion in the environment.

Owing to the wide range of applications, studies of natural convection flow and heat transfer have been vigorously pursued for many years. Experimental investigations of cavity flows driven by lateral heating have been reported by Elder [1], Imberger [2], and more recently by Patterson and Imberger [3], Simpkins and Chen [4], Armfield [5] and Patterson [6]. In general, these flows consist of a main circulation in which fluid rises at the hot wall, sinks at the cold wall, and travels laterally across the intervening core region.

Extensive numerical results have been obtained by researchers during the past twenty-five years for cavity flows of different aspect ratio L (length/height), Rayleigh number R and Prandtl number σ. Quon [7] carried out finite difference computations for convection in a square cavity for a variety of dynamical boundary conditions, Rayleigh numbers and Prandtl numbers. Cormack *et al.* [8] obtained numerical solutions in shallow cavities for a variety of Rayleigh numbers while de Vahl Davis and Mallinson [9] studied the stability and transition of tall cavity flows numerically. A comparative numerical study of convection flows in a square cavity was described by de Vahl Davis and Jones [10]. More detailed numerical studies of cavity flows have been carried out by Vest and Arpaci [11] and Bejan and Tien [12], while Shiralkar *et al.* [13] investigated numerically the high Rayleigh number regime. Drummond and Korpela [14] have discussed numerical results for a shallow cavity with a variety of Rayleigh numbers and Prandtl numbers and further numerical studies have been carried out by Gaskell and Wright [15], and Winters [16].

For a shallow cavity ($L \to \infty$) and Rayleigh numbers $R \ll L$ the flow is dominated by conduction and consists of a Hadley cell driven by the constant horizontal temperature gradient set up between the end walls. Cormack *et al.* [17] predicted that the flow consists of two distinct parts: a parallel flow in the core region which extends for most of the length of the cavity and a second, non-parallel flow near the ends. Non-linear convective effects first become significant at the ends of the cavity where the flow is turned when $R_1 = R/L = O(1)$. Hart [18] found that for small σ the Hadley cell is susceptible to a variety of instabilities. For Rayleigh numbers greater than a critical value $R_1 = R_{1c}(\sigma)$ the parallel core flow is destroyed and replaced by stationary multiple cells (Daniels *et al.* [19]). These transverse rolls are actually an integral part of the steady-state solution in the cavity, unlike the longitudinal and time-dependent instabilities which may also occur. Their existence was confirmed by numerical simulations of the end-zone flow at low Prandtl numbers by Hart [20]. During recent years, new work has focused on the nonlinear end-zone structure in cases where the multiple-cell instability is avoided. Then, as the Rayleigh number increases, the extent of the end-zones increases and as $R_1 \to \infty$ a complicated asymptotic structure develops. For the case where the horizontal walls of the cavity are perfectly conducting, certain properties of the end-zone solution for $R_1 = O(1)$ have been discussed by Gargaro [21] but little analytical progress has been made in identifying the limiting structure of the solution as $R_1 \to \infty$. The above problem is typical of a wide class of 'end-zone' problems where solutions of the governing equations and boundary conditions generally require a numerical approach.

NOMENCLATURE

h	height of cavity
l	length of cavity
L	aspect ratio of cavity, l/h
Nu	Nusselt number
R	Rayleigh number
R_1	scaled Rayleigh number
T^*	dimensional temperature
$\bar{T}$, T	non-dimensional temperature
x^*, z^*	dimensional coordinates
x, z	non-dimensional coordinates
u^*, w^*	dimensional velocity components.

Greek symbols

α	wave number
β	coefficient of thermal expansion
κ	thermal diffusivity
ν	kinematic viscosity
σ	Prandtl number
$\bar{\psi}$, ψ	non-dimensional stream function
$\bar{\omega}$, ω	non-dimensional vorticity function.

This paper describes numerical solutions of the full nonlinear Boussinesq equations in the end-zone for the case of conducting horizontal boundaries and for a range of Rayleigh numbers. Results are obtained for both low Prandtl number ($\sigma = 0.05$) and for the case of air ($\sigma = 0.733$) and are compared with the stability theory of Hart [18] for which refined calculations have been reported in refs. [21–25].

2. FORMULATION

The cavity is defined by the region $0 \leqslant x^* \leqslant l$, $0 \leqslant z^* \leqslant h$, with the vertical sidewalls $x^* = 0$ and $x^* = l$ maintained at constant temperatures T_0 and $T_0 + \Delta T$, respectively. Non-dimensional variables of temperature, velocity, length and time are defined by

$$T^* = T_0 + \Delta T \bar{T}(x, z, t), \tag{1}$$

$$(u^*, w^*) = \frac{\kappa(\bar{u}, \bar{w})}{h}, \tag{2}$$

$$(x^*, z^*) = h(x, z), \tag{3}$$

$$t^* = \frac{h^2}{\kappa} t, \tag{4}$$

where κ is the thermal diffusivity. By defining a stream function $\bar{\psi}$ such that

$$\bar{u} = \frac{\partial \bar{\psi}}{\partial z}, \quad \bar{w} = -\frac{\partial \bar{\psi}}{\partial x}, \tag{5}$$

the governing equations, subject to the Boussinesq approximation, can be written in non-dimensional form as

$$\sigma^{-1}\left(\frac{\partial \bar{\omega}}{\partial t} + J(\bar{\omega}, \bar{\psi})\right) = \nabla^2 \bar{\omega} + R\frac{\partial \bar{T}}{\partial x}, \tag{6}$$

$$\nabla^2 \bar{\psi} = -\bar{\omega}, \tag{7}$$

$$\frac{\partial \bar{T}}{\partial t} + J(\bar{T}, \bar{\psi}) = \nabla^2 \bar{T}, \tag{8}$$

where the Prandtl number σ and the Rayleigh number R are defined by

$$\sigma = \frac{\nu}{\kappa}, \quad R = \frac{g\beta\Delta T h^3}{\kappa\nu} \tag{9}$$

and $\bar{\omega}$ is the vorticity. Here ν is the kinematic viscosity, β is the coefficient of thermal expansion, and g is the acceleration due to gravity.

The boundary conditions on the vertical end walls are

$$\bar{\psi} = \frac{\partial \bar{\psi}}{\partial x} = 0 \quad \text{on} \quad x = 0, L, \tag{10}$$

$$\bar{T} = 0 \quad \text{on} \quad x = 0. \tag{11}$$

$$\bar{T} = 1 \quad \text{on} \quad x = L, \tag{12}$$

and the rigid horizontal surfaces are assumed to be conducting so that

$$\bar{\psi} = \frac{\partial \bar{\psi}}{\partial z} = 0 \quad \text{on} \quad z = 0, 1, \tag{13}$$

$$\bar{T} = \frac{x}{L} \quad \text{on} \quad z = 0, 1 \tag{14}$$

where $L = l/h$ is the cavity aspect ratio.

These equations and boundary conditions have solutions which possess the centrosymmetric properties

$$\left.\begin{aligned} \bar{\psi}(x, z, t) &= \bar{\psi}(L-x, 1-z, t), \\ \bar{T}(x, z, t) &= 1 - \bar{T}(L-x, 1-z, t), \\ \bar{\omega}(x, z, t) &= \bar{\omega}(L-x, 1-z, t), \end{aligned}\right\} \tag{15}$$

so that in general for the steady-state solution only half of the flow domain needs to be considered. The motion is controlled by the three parameters σ, R and L. The Hadley regime, defined by $L \to \infty$ with fixed R, has been discussed in detail by Cormack *et al.* [17]. It can be shown that their approach fails when $R = O(L)$ (Daniels *et al.* [19]), and the present work is concerned with the distinguished limit $L \to \infty$ such that

$$R_1 = \frac{R}{L} = O(1). \tag{16}$$

Unlike the Hadley structure these flows contain strong nonlinear effects in the end regions.

3. CORE SOLUTION AND END-ZONE STRUCTURE

Away from the end walls it is appropriate to use as independent variables,

$$\xi = \frac{x}{L}, \quad z = z \tag{17}$$

and the steady-state solution is found by expanding formally the stream function and the temperature as

$$\left.\begin{aligned}\bar{\psi} &= \psi_0(\xi, z) + L^{-1}\psi_1(\xi, z) + O(L^{-2}) \\ \bar{T} &= T_0(\xi, z) + L^{-1}T_1(\xi, z) + O(L^{-2})\end{aligned}\right\} (L \to \infty). \tag{18}$$

Substituting into (6)–(8), and using the centro-symmetry relations together with the requirement that

$$T_0 = 0 \quad \text{at} \quad \xi = 0 \tag{19}$$

gives at leading order

$$T_0 = \xi, \quad \psi_0 = R_1 F(z) \tag{20}$$

and at second order

$$T_1 = R_1 G(z) \tag{21}$$

where

$$F(z) = \frac{z^2}{24}(1-z)^2 \tag{22}$$

and

$$G(z) = \frac{z^5}{120} - \frac{1}{48}z^4 + \frac{1}{72}z^3 - \frac{1}{720}z. \tag{23}$$

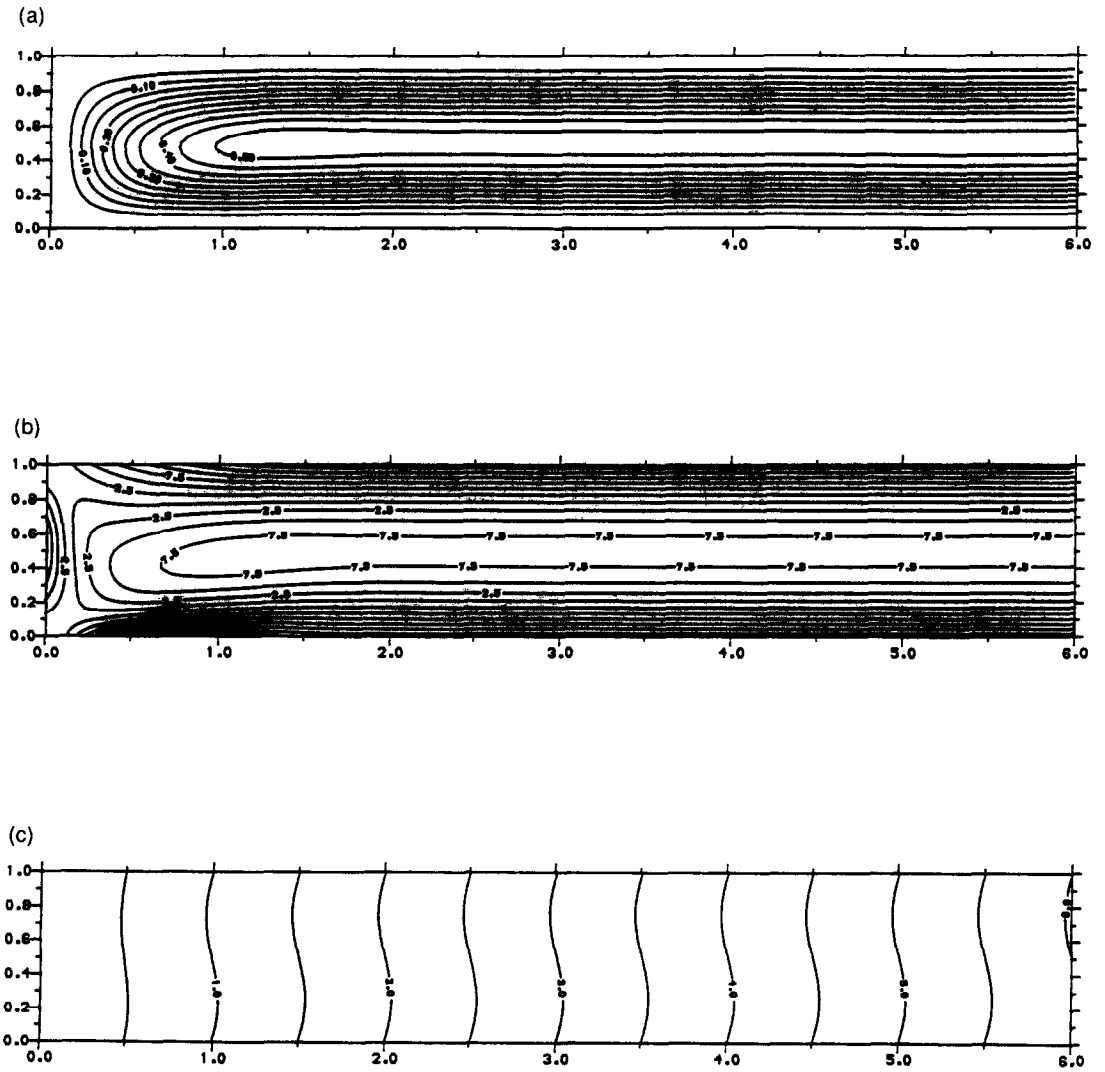

FIG. 1. Contours of the steady-state solution for (a) stream function, (b) vorticity, (c) temperature, for $\sigma = 0.05$ and $R_1 = 200$, using a 180×30 computational grid with $x_\infty = 6$.

Thus in the core region

$$\left.\begin{aligned}\bar{\psi} &\sim R_1 F(z)\\ \bar{T} &\sim \xi + L^{-1} R_1 G(z)\end{aligned}\right\} \quad (L \to \infty) \tag{24}$$

and this solution is actually an exact steady-state solution of the full equations (6)–(8). It represents a horizontal two-way flow with fluid moving towards the cold wall in the top half of the cavity ($z > 1/2$) and the hot wall in the bottom half ($z < 1/2$). The temperature field varies linearly with ξ and is also vertically stratified. Near the ends of the cavity the fluid must be turned and the solution (20) is clearly invalid. Indeed, the core solution is only valid if a consistent solution can be found in end-regions near each vertical wall.

Since the overall motion can be assumed centrosymmetric only the solution at the cold end of the cavity needs to be considered, where the temperature and stream function can be expanded in the form

$$\bar{T} = L^{-1} T(x, z, t) + \cdots, \quad \bar{\psi} = \psi(x, z, t) + \cdots,$$
$$\bar{\omega} = \omega(x, z, t) + \cdots. \tag{25}$$

It then follows from (6)–(14) that the motion is governed by the full nonlinear Boussinesq equations

$$\sigma^{-1}\left(\frac{\partial \omega}{\partial t} + J(\omega, \psi)\right) = \nabla^2 \omega + R_1 \frac{\partial T}{\partial x}, \tag{26}$$

$$\nabla^2 \psi = -\omega, \tag{27}$$

$$\frac{\partial T}{\partial t} + J(T, \psi) = \nabla^2 T, \tag{28}$$

in the region $x \geq 0$, $0 \leq z \leq 1$ with boundary conditions

$$\psi = \frac{\partial \psi}{\partial z} = 0, \quad T = x \quad \text{on} \quad z = 0, 1. \tag{29}$$

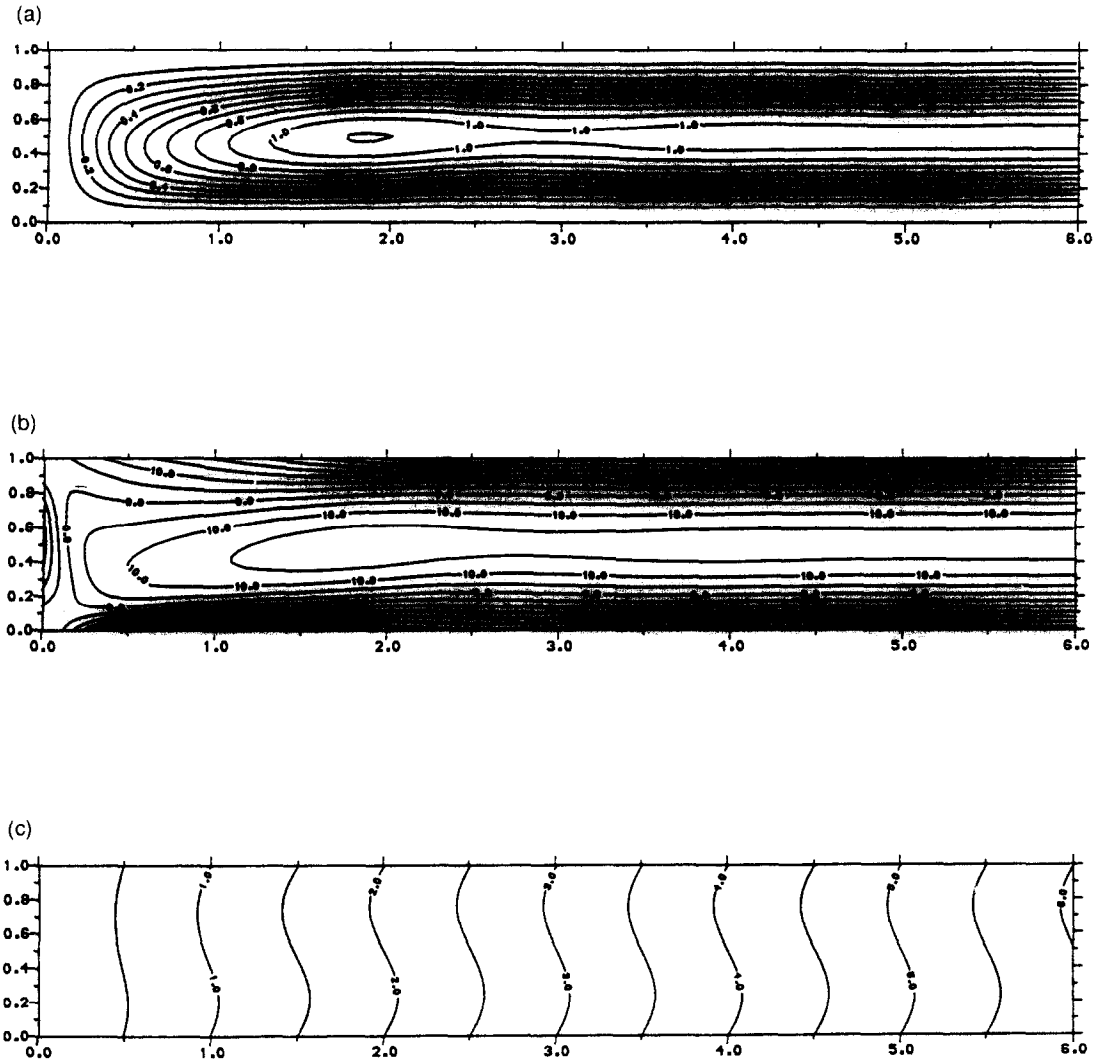

FIG. 2. Contours of the steady-state solution for (a) stream function, (b) vorticity, (c) temperature, for $\sigma = 0.05$ and $R_1 = 400$, using a 180×30 computational grid with $x_\infty = 6$.

$$\psi = \frac{\partial \psi}{\partial x} = T = 0 \quad \text{on} \quad x = 0, \tag{30}$$

and

$$\psi \to R_1 F(z), \quad T \sim x + R_1 G(z) \quad (x \to \infty). \tag{31}$$

Here (29) and (30) are the relevant boundary conditions on the cavity walls while (31) ensures that the solution matches with that in the core. Thus the regime where R_1 is $O(1)$ is identified by the presence of nonlinear inertial and convective effects in roughly square zones at each end of the cavity and the flow is determined by the solution of the full Boussinesq system (26)–(31), which in general needs to be solved by a numerical technique. This is considered in the next section.

Certain properties of the end-zone problem have been studied by Gargaro [21] who considered the manner in which the steady solution approaches the parallel core flow (24). This is found by considering the forms

$$\left.\begin{aligned} \psi &\sim R_1 F(z) + \phi(z) \exp(-\alpha x) \\ T &\sim x + R_1 G(z) + \theta(z) \exp(-\alpha x) \end{aligned}\right\} \quad (x \to \infty). \tag{32}$$

Substitution into (26)–(28) shows that the eigenvalue α is determined by the solution of the system

$$\phi'''' + 2\alpha^2 \phi'' + \alpha^4 \phi + \alpha R_1 \theta = \alpha R_1 (F''' \phi - F'(\phi'' + \alpha^2 \phi))/\sigma \tag{33}$$

$$\theta'' + \alpha^2 \theta - \phi' = \alpha R_1 (G' \phi - F' \theta) \tag{34}$$

with

$$\theta = \phi = \phi' = 0 \quad \text{on} \quad z = 0, 1. \tag{35}$$

A triply-infinite family of eigenvalues α with positive real part is found to exist for $R_1 < R_{1c}(\sigma)$, indicating

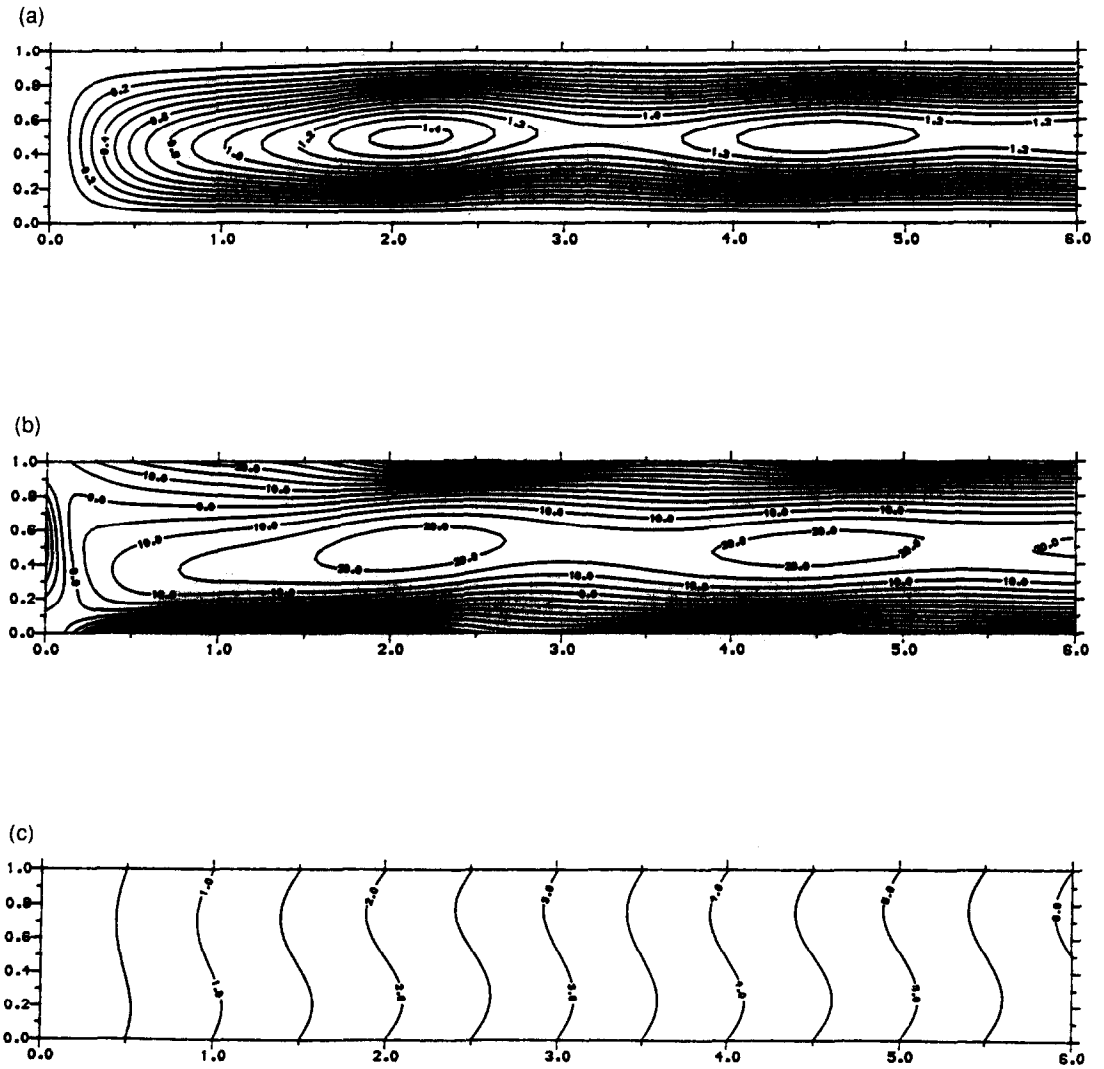

FIG. 3. Contours of the steady-state solution for (a) stream function, (b) vorticity, (c) temperature, for $\sigma = 0.05$ and $R_1 = 500$, using a 180×30 computational grid with $x_\infty = 6$.

that an end-zone solution can then be found consistent with exponential decay to the parallel core flow. At the critical Rayleigh number R_{1c}, the real part of the leading eigenvalue tends to zero, leaving a purely imaginary solution $\alpha = i\alpha_c$, equivalent to oscillatory behaviour associated with instability of the parallel core flow in the form of transverse rolls (Hart [18]), and for $R_1 > R_{1c}(\sigma)$, the parallel flow is destroyed by multiple eddies which are forced into the core from the end-zones. The function $R_{1c}(\sigma)$ is given by Gargaro [21] and exists only in the region $0 \leqslant \sigma \leqslant 0.27$, tending to infinity as $\sigma \to 0.27$ and approaching 7980σ as $\sigma \to 0$ (Hart [18]). For $\sigma > 0.27$ an end-zone solution consistent with a smooth approach (31) to a parallel core flow is possible for any Rayleigh number R_1. For lower Prandtl numbers the outer behaviour (31) is only possible when $R_1 < R_{1c}(\sigma)$.

For low Rayleigh numbers $R_1 \to 0$, the steady solution of the end zone problem can be developed as a power series in R_1 in the manner described by Cormack *et al.* [17]. In this case

$$T = x + R_1 T_1(x, z) + \cdots, \quad \psi = R_1 \psi_1(x, z) + \cdots \tag{36}$$

where ψ_1 satisfies the equation

$$\nabla^4 \psi_1 = 1 \tag{37}$$

with boundary conditions

$$\psi_1 = \frac{\partial \psi_1}{\partial z} = 0, \quad z = 0, 1, \tag{38}$$

$$\psi_1 = \frac{\partial \psi_1}{\partial x} = 0, \quad x = 0, \tag{39}$$

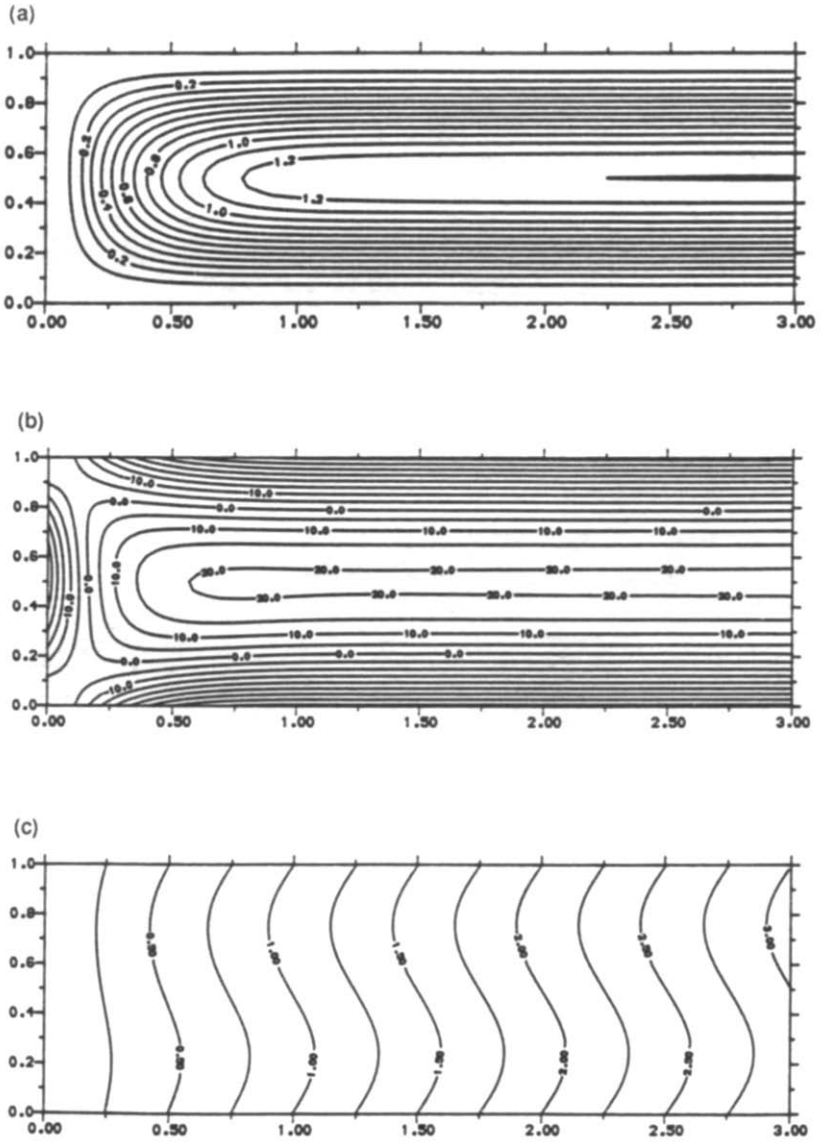

FIG. 4. Contours of the steady-state solution for (a) stream function, (b) vorticity, (c) temperature, for $\sigma = 0.733$ and $R_1 = 500$, using a 90×30 computational grid with $x_\infty = 3$.

$$\psi_1 \to F(z) \quad (x \to \infty). \tag{40}$$

The solution given by Cormack *et al.* [17] is equivalent to a symmetric turning motion.

4. NUMERICAL SCHEME FOR THE END-ZONE PROBLEM

In order to solve the system (26)–(31) numerically, a finite difference method is considered. For evolution equations, Crank–Nicolson and Peaceman–Rachford methods have been used extensively, but more recently another method called the Dufort–Frankel method, as outlined in ref. [26], has been developed. Like the Crank–Nicolson and Peaceman–Rachford methods, it has second-order accuracy but since it is an explicit method, it must meet the Courant condition to achieve numerical stability. Although the size of the time step is restricted by this condition, it is still a very effective and fast method.

For elliptic equations, a five-point scheme can be adopted in which centred differences are used to approximate the original partial differential equation. Convergence of the Successive Over-Relaxation can be improved by use of fine and coarse grids within a Multigrid scheme (Brandt [27]). Here the Dufort–Frankel method is used to solve the evolution equations (26), (28), and the Multilevel method to solve the Poisson equation (27). The outer form (31) at $x = \infty$ is handled by a finite truncation of x so that the conditions

$$\frac{\partial T}{\partial x} = 1, \quad \psi = R_1 F(z), \tag{41}$$

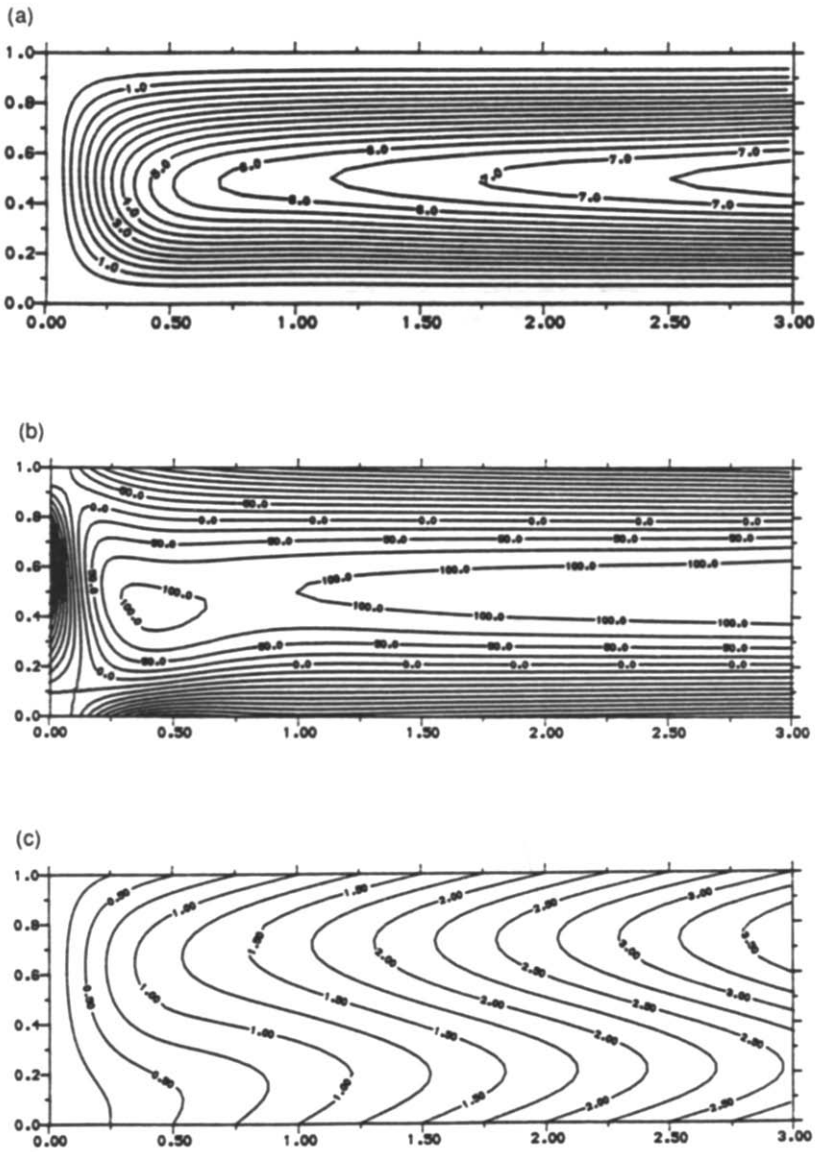

FIG. 5. Contours of the steady-state solution for (a) stream function, (b) vorticity, (c) temperature, for $\sigma = 0.733$ and $R_1 = 3000$, using a 90×30 computational grid with $x_\infty = 3$.

are applied in the computational domain at $x = x_\infty < \infty$. It is then necessary to ensure that x_∞ is chosen sufficiently large that the computed solution does indeed approximate the actual solution of (26)–(31). The main interest is in the steady-state solution, and the computation is stopped when the maximum difference between values of the solution at successive time steps is less than a specified tolerance, usually taken to be 10^{-6} for the temperature and vorticity fields. Further details of the numerical techniques involved in solving the whole system are discussed by Wang [28].

For a steady-state solution, integration of the heat equation over the end zone gives

$$\int_0^{x_\infty}\int_0^1 \nabla^2 T \, dx \, dz = \int_0^{x_\infty}\int_0^1 \frac{\partial(T,\psi)}{\partial(x,z)} dx \, dz, \quad (42)$$

and using the outer form (31) gives

$$\int_0^1 \left.\frac{\partial T}{\partial x}\right|_{x=0} dz - \int_0^{x_\infty} \left(\left.\frac{\partial T}{\partial z}\right|_{z=1} - \left.\frac{\partial T}{\partial z}\right|_{z=0}\right) dx = 1 + \int_0^1 \psi \left.\frac{\partial T}{\partial z}\right|_{x=x_\infty} dz = 1 + \frac{R_1^2}{1\,209\,600}. \quad (43)$$

Once a steady-state numerical solution of the end zone is obtained, the integrals on the left hand side of equation (43) can be calculated using Simpson's rule. The above relation can then be used to provide a check on the accuracy of the numerical solution.

5. NUMERICAL RESULTS AND DISCUSSION

This section presents the results of numerical calculations of the end zone solution for two Prandtl numbers, $\sigma = 0.05$ and $\sigma = 0.733$, and for a range of Rayleigh numbers, R_1. The outer boundary x_∞ is

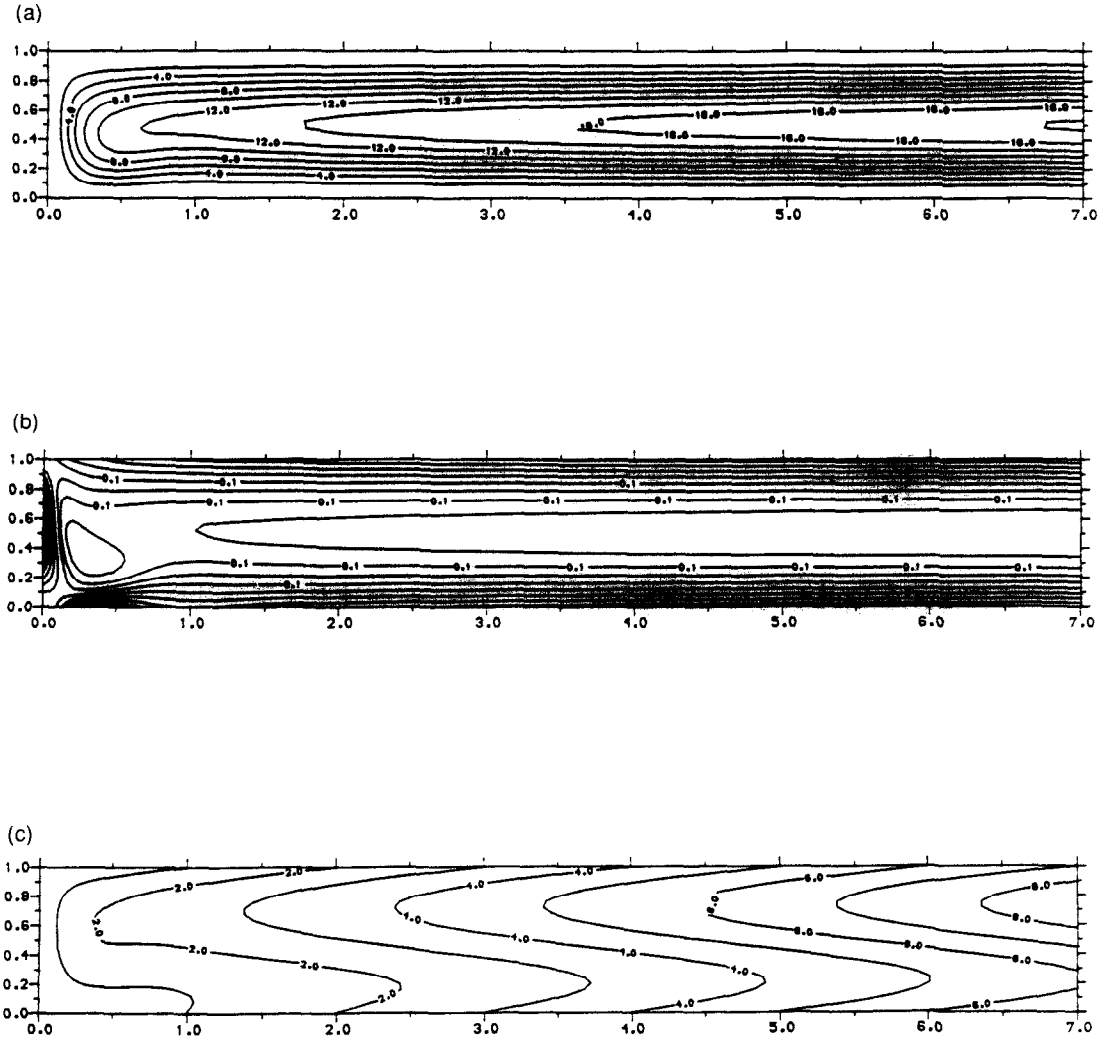

FIG. 6. Contours of the steady-state solution for (a) stream function, (b) vorticity, (c) temperature, for $\sigma = 0.733$ and $R_1 = 7000$, using a 175×25 computational grid with $x_\infty = 7$.

varied according to the value of the Rayleigh number in order to accommodate the outer boundary condition (31).

Gargaro's analysis [21] indicates that in the absence of multicellular motion ($\sigma > 0.27$) the leading eigenvalue α which determines the decay rate of the end zone solution as $x \to \infty$ is of order R_1^{-1} as $R_1 \to \infty$. Thus the lateral extent of the end zone is proportional to R_1, necessitating the use of an extensive computational domain at large Rayleigh numbers.

For low Prandtl number ($\sigma = 0.05$) there is the possibility of spatial oscillations when the Rayleigh number R_1 reaches the critical value $R_{1c}(0.05) \approx 455$ (Gargaro [21]). Contour plots of stream function, vorticity and temperature with $\sigma = 0.05$ and Rayleigh numbers ranging from 200 to 500 are shown in Figs. 1–3. Here, an outer boundary $x_\infty = 6$ is used. Figure 1 shows the near-symmetric flow associated with the low Rayleigh number limit (36); the temperature field is primarily linear in x together with a small vertical gradient associated with the term $R_1 G(z)$. In Fig. 2, where the Rayleigh number is increased to 400, the streamline field indicates the development of weak eddies along $z = 0.5$. This secondary flow increases in amplitude as the Rayleigh number increases, as shown for $R_1 = 500$ in Fig. 3. The critical wavelength predicted by linear stability theory at $R_{1c} = 455$ is $z = 2\pi/\alpha_c = 2.33$, consistent with the evidence of the numerical results obtained here. The results are also in good agreement with those obtained by Drummond and Korpela [14] by solving the full cavity problem for a range of large aspect ratios.

Numerical results have been obtained for air ($\sigma = 0.733$) for a range of Rayleigh numbers from 500 to 14000. Outer boundaries varying from $x_\infty = 3$ to 7 were chosen for these computations. Figures 4–7 illustrate the contour fields of stream function, vorticity and temperature in the end region. These are

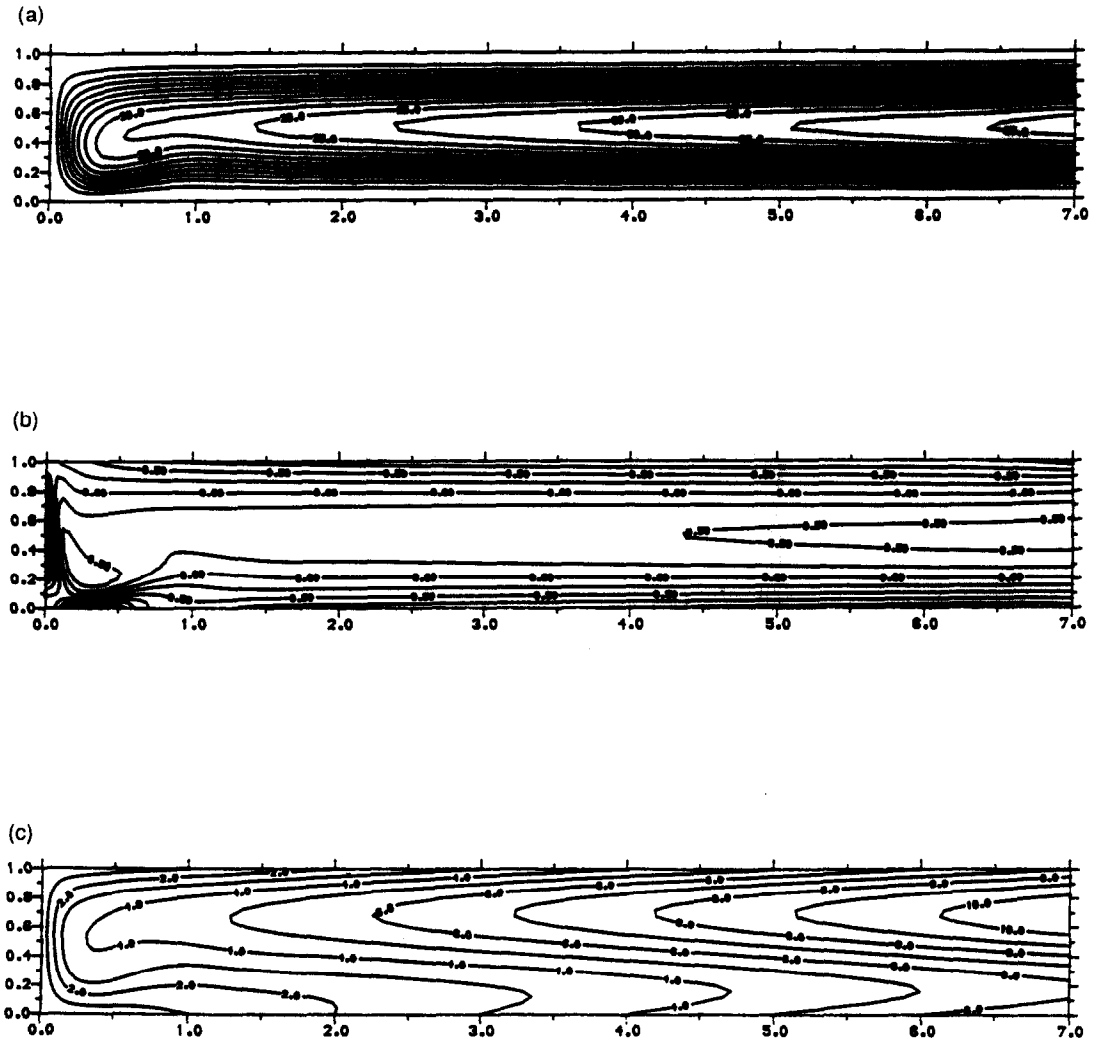

FIG. 7. Contours of the steady-state solution for (a) stream function, (b) vorticity, (c) temperature, for $\sigma = 0.733$ and $R_1 = 14000$, using a 175×25 computational grid with $x_\infty = 7$.

quite different from those with $\sigma = 0.05$ and, in particular, the flow is free from multiple eddies since $\sigma > 0.27$. In Fig. 4, where $R_1 = 500$, the flow approximates the symmetric low Rayleigh number form (36) and the main turning motion occurs in the region $0 \leqslant x < 1$ close to the cold wall. As the Rayleigh number is increased, an inward penetration of nonlinear convective effects from the end of the cavity is observed. The non-parallel region extends into the cavity, as shown in the results for $3000 \leqslant R_1 \leqslant 14000$ in Figs. 5–7. The vertical temperature variation increases and there is a tendency for the turning

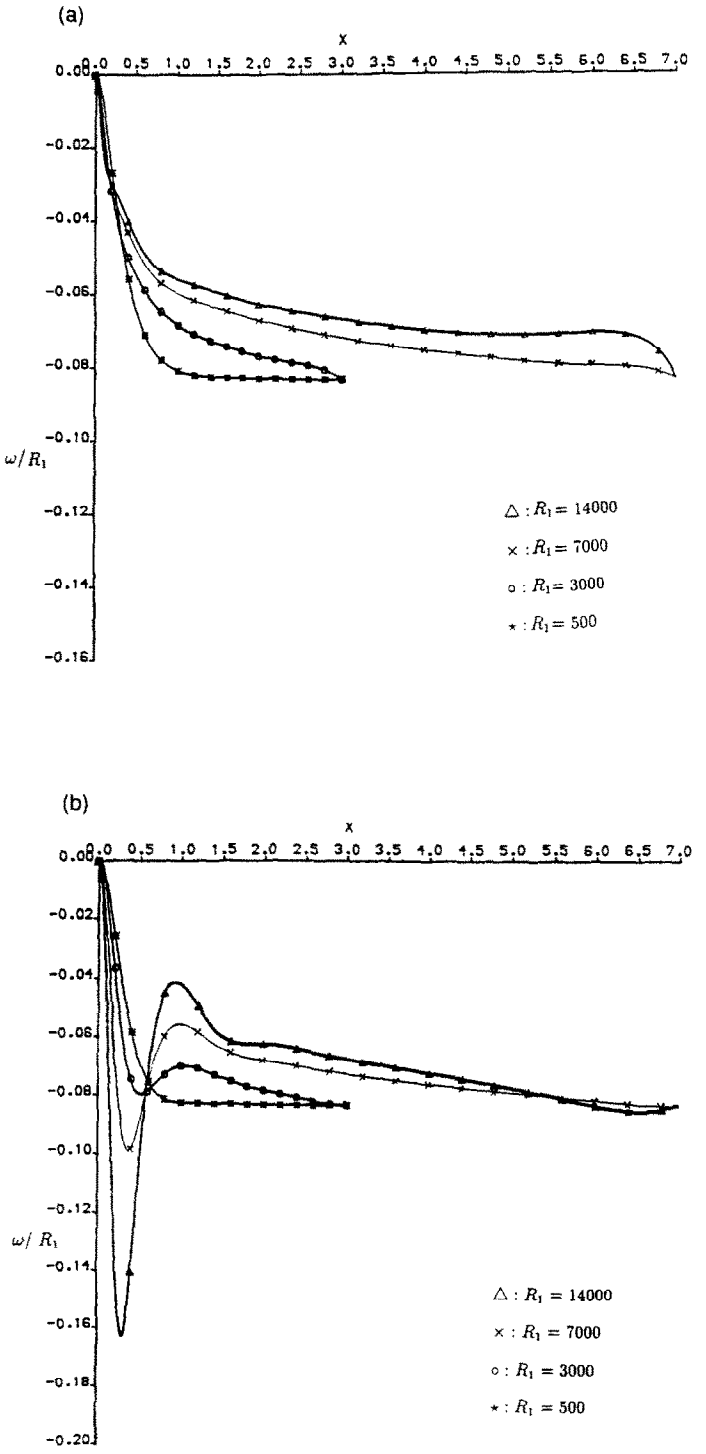

FIG. 8. The skin friction ω/R_1 with $\sigma = 0.733$ for different Rayleigh numbers on the horizontal walls: (a) top wall, (b) bottom wall.

motion to dip towards the lower boundary near the cold wall. Profiles of the skin friction on the horizontal walls (Fig. 8) show a sharp change on the lower boundary close to the cold wall and at higher Rayleigh numbers there is a further sharp decrease just downstream, suggesting the possibility of a flow separation on the bottom wall at sufficiently high Rayleigh numbers.

Figure 9 shows the skin friction and the local Nusselt number on the cold wall and local Nusselt numbers for the horizontal walls are shown in Fig. 10. The heat flux changes remarkably little on the top wall for

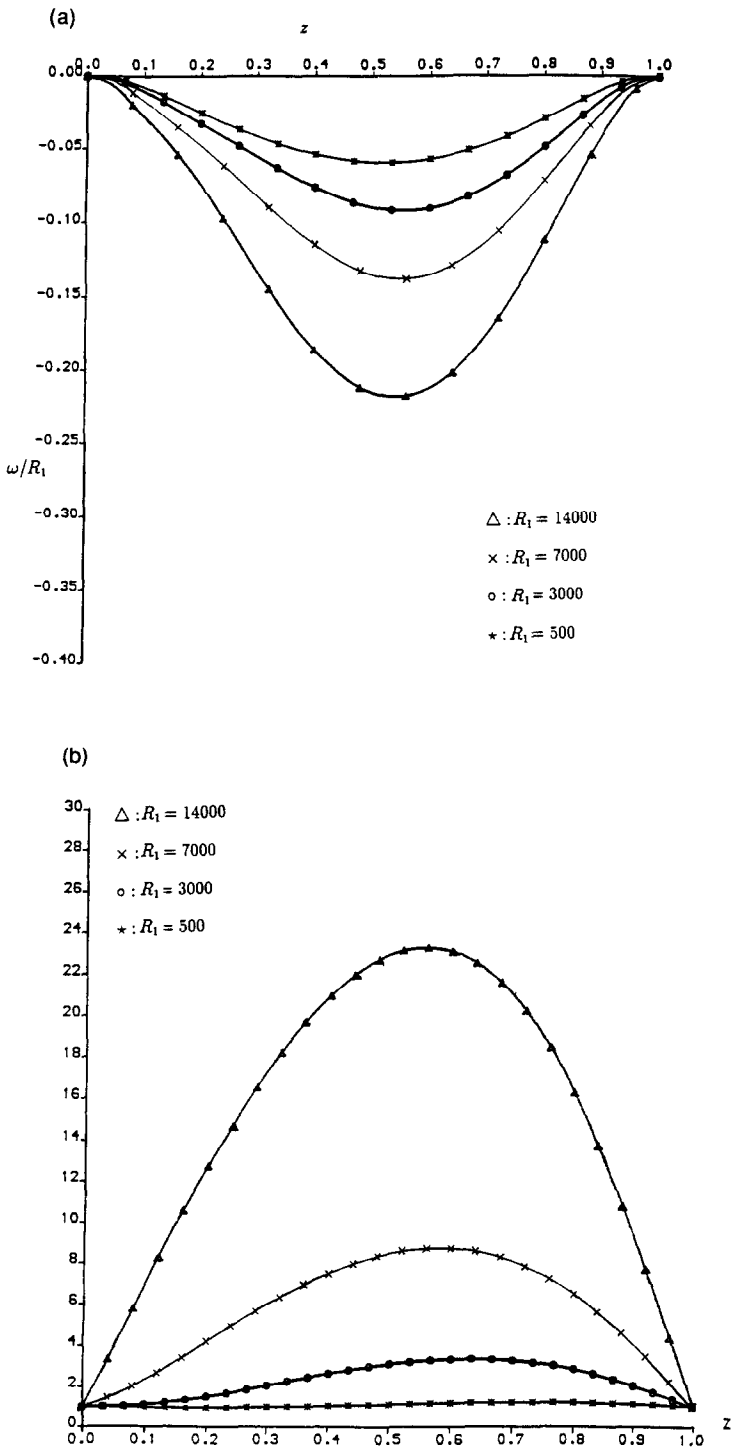

FIG. 9. The profiles of (a) skin friction ω/R_1 and (b) local Nusselt number $\partial T/\partial x|_{x=0}$ with $\sigma = 0.733$ for different Rayleigh numbers on the cold wall.

different Rayleigh numbers, but on the bottom wall, there are significant changes near the cold corner where heat is transferred out of the cavity for Rayleigh numbers greater than about 3000. The behaviour of the local Nusselt number on the cold wall indicates how the outward heat transfer is significantly enhanced as R_1 increases; the overall Nusselt number for the cold wall is given in Table 1. Formula (43) was used to test the accuracy of the numerical results, and values of each side of the equation are listed in Table 2. This indicates good consistency, discrepancies being attributable to the limitation in the number of grid points and the finite extent of the outer boundary at $x = x_\infty$.

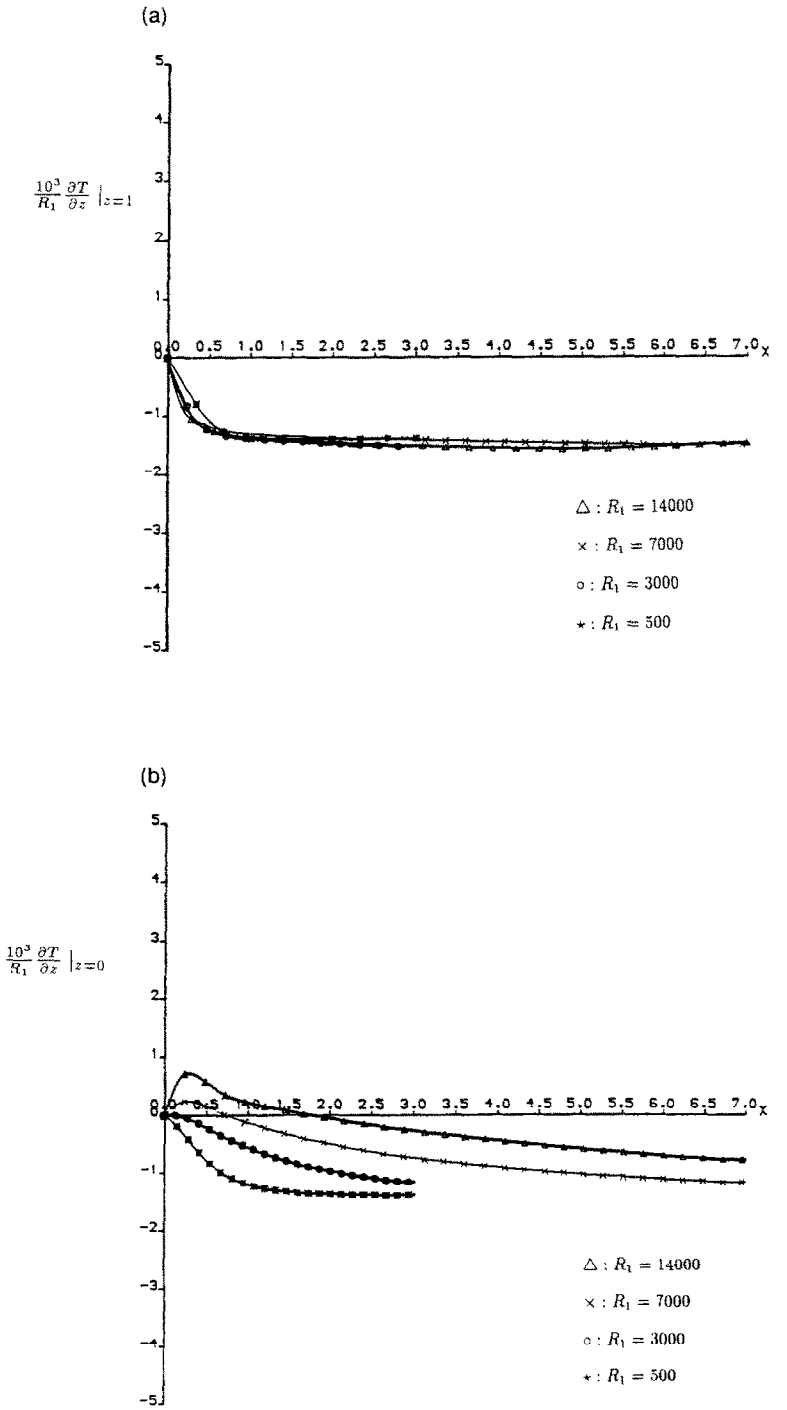

FIG. 10. The local Nusselt number $\partial T/\partial z$ with $\sigma = 0.733$ for different Rayleigh numbers on the horizontal walls: (a) top wall, (b) bottom wall.

Table 1. The overall Nusselt number at the cold wall for air

R_1	$\int_0^1 \left.\frac{\partial T}{\partial x}\right\|_{x=0} dz$
500	1.0733
3000	2.3418
7000	5.7074
14000	15.2633

Table 2. Comparison of the two sides of equation (43) for different Rayleigh numbers and Prandtl numbers

R_1	σ	Left-hand side	Right-hand side	Discrepancy
500	0.733	1.22624	1.20668	0.01956
3000	0.733	8.06246	8.44047	−0.37801
7000	0.733	39.1836	41.5092	−2.3256
14000	0.733	130.48	163.037	−32.557
200	0.05	1.05495	1.03307	0.02188
400	0.05	1.15291	1.13227	0.02064
500	0.05	1.22333	1.20667	0.0166
600	0.05	1.28574	1.29761	−0.01187

In conclusion, the present numerical results confirm predictions of the onset of low Prandtl number multicellular convection and at higher Prandtl numbers shed light on the nonlinear development of the flow with increasing Rayleigh number. In particular the results confirm the outward penetration of non-parallel effects on a scale proportional to the Rayleigh number and the development of thin boundary-layer structures near the walls of the cavity. In addition, the results for the Nusselt number determine the influence of convection in the end-zones on the lateral heat transfer across the cavity for a range of values of the scaled Rayleigh number $R_1 = R/L$.

REFERENCES

1. J. W. Elder, Laminar free convection in a vertical slot, *J. Fluid Mech.* **23,** 77–98 (1965).
2. J. Imberger, Natural convection in a shallow cavity with differentially heated end walls. Part 3. Experimental results, *J. Fluid Mech.* **65,** 247–260 (1974).
3. J. C. Patterson and J. Imberger, Unsteady natural convection in a rectangular cavity, *J. Fluid Mech.* **100,** 65–86 (1980).
4. P. G. Simpkins and K. S. Chen, Convection in horizontal cavities, *J. Fluid Mech.* **166,** 21–39 (1986).
5. S. W. Armfield, Direct simulation of unsteady natural convection in a cavity. In *3rd Int. Symp. on Computational Fluid Dynamics*, pp. 305–310. North-Holland, Amsterdam (1989).
6. J. C. Patterson, Experiments in unsteady natural convection. In *Proc. Fourth Australasian Conference on Heat and Mass Transfer*, pp. 299–306, Christchurch (1989).
7. C. Quon, High Rayleigh number convection in an enclosure—a numerical study, *Phys. Fluids* **15,** 12–19 (1972).
8. D. E. Cormack, L. G. Leal and J. H. Seinfeld, Natural convection in a shallow cavity with differentially heated end walls. Part 2. Numerical solutions, *J. Fluid Mech.* **65,** 231–246 (1974).
9. G. de Vahl Davis and G. D. Mallinson, A note on natural convection in a vertical slot, *J. Fluid Mech.* **72,** 87–93 (1975).
10. G. de Vahl Davis and I. P. Jones, Natural convection in a square cavity: a comparison exercise, *Int. J. Numer. Methods Fluids* **3,** 227–248 (1983).
11. C. M. Vest and V. S. Arpaci, Stability of natural convection in a vertical slot, *J. Fluid Mech.* **36,** 1–15 (1969).
12. A. Bejan and C. L. Tien, Laminar natural convection heat transfer in a horizontal cavity with different end temperatures, *Trans. A.S.M.E. J. Heat Transfer* **100,** 641–647 (1978).
13. G. Shiralkar, A. Gadgil and C. L. Tien, High Rayleigh number convection in a shallow enclosure with different end temperatures, *Int. J. Heat Mass Transfer* **24,** 1621–1629 (1981).
14. J. E. Drummond and S. A. Korpela, Natural convection in a shallow cavity, *J. Fluid Mech.* **182,** 543–564 (1987).
15. P. H. Gaskell and N. G. Wright, A multigrid algorithm for the investigation of thermal recirculating fluid flow problems. In *5th Int. Conf. on Num. Meth. for Thermal Problems*, Montreal, Canada (1987).
16. K. H. Winters, Laminar natural convection in a partially divided rectangular cavity at high Rayleigh number, *J. Numer. Methods Fluids* **8,** 247–281 (1988).
17. D. E. Cormack, L. G. Leal and J. Imberger, Natural convection in a shallow cavity with differentially heated end walls. Part 1. Asymptotic theory, *J. Fluid Mech.* **65,** 209–229 (1974).
18. J. E. Hart, Stability of thin non-rotating Hadley circulations, *J. Atmos. Sci.* **29,** 687–697 (1972).
19. P. G. Daniels, P. A. Blythe and P. G. Simpkins, Onset of multicellular convection in a shallow laterally heated cavity, *Proc. R. Soc. A* **411,** 327–350 (1987).
20. J. E. Hart, Low Prandtl number convection between differentially heated end walls, *Int. J. Heat Mass Transfer* **26,** 1069–1074 (1983).
21. R. J. Gargaro, Convection in a shallow laterally heated cavity with conducting boundaries, *J. Engng Math.* **25,** 99–113 (1991).
22. J. E. Hart, A note on stability of low Prandtl number Hadley circulation, *J. Fluid Mech.* **132,** 271–281 (1983).
23. H. P. Kuo and S. A. Korpela, Stability and finite amplitude natural convection in a shallow cavity with insulated top and bottom and heated from a side, *Phys. Fluids* **31,** 33–42 (1988).
24. T. M. Wang and S. A. Korpela, Convection rolls in a shallow cavity heated from a side, *Phys. Fluids A* **1,** 947–953 (1989).
25. T. M. Wang and S. A. Korpela, Secondary instabilities of convection in a shallow cavity, *J. Fluid Mech.* **234,** 147–170 (1992).
26. P. J. Roache, *Computational Fluid Dynamics*. Hermosa, Alberquerque, NM (1976).
27. A Brandt, Multi-level adaptive solutions to boundary-value problems, *Math. Comp.* **31,** 333–390 (1977).
28. P. Wang, Thermal convection in slender laterally-heated cavities, Ph.D. Dissertation, City University, London (1992).